



ISSN: 0067-2904

## Copper Molarity Effect on the Optical Properties of $\text{Cu}_2\text{CdSnS}_4$ Quaternary Thin Films

Shaymaa Khashea Abdo, Jamal M. Rzaij\*

Department of Physics, College of Science, University of Anbar, Ramadi, Iraq

Received: 19/5/2020

Accepted: 10/8/2020

### Abstract

The quaternary alloy of  $\text{Cu}_2\text{CdSnS}_4$  (CCSS) is one type of thin film materials that contributes to the field of photovoltaic devices manufacturing, the importance of which has not been commonly enlightened as most of the other materials. For the preparation of CCSS thin films at 350 °C on glass substrates, the chemical spray pyrolysis technique was used. The optical properties of thin films prepared under the influence of the variation of copper solution molarity (0.03, 0.05, 0.07, and 0.09 M) on the quaternary compound were examined using a UV-vis spectrophotometer. The findings of the AFM study showed the atoms on the surface that are acclimatized in the form of nanorods with an increase in the average grain size from 62.72 to 79.17 nm. The results also showed an improvement in the average surface roughness from 5.69 to 12.8 nm when copper concentration increased from 0.03 to 0.09 M. The UV-vis results showed that the optical transmittance of CCSS decreases by increasing the solution molarity of copper, with a change in the absorption edge toward the low energy side (redshift). With an increase in the wavelength between 725 and 960 nm, a low absorption coefficient was found in the infrared region, while a strong absorption coefficient in the visible range was observed with the increase in copper solution molarity. The energy gap values decreased from 1.6 to 1.47 eV when copper solution molarity increased from 0.03 to 0.09 M. By raising copper solution molarity to 0.09 M, the refractive index at the absorption edge was increased from 1.6 to 1.97, while the extinction coefficient reduced.

**Keywords:** copper, optical properties,  $\text{Cu}_2\text{CdSnS}_4$ , thin films, spray pyrolysis

### تأثير تركيز مولارية محلول النحاس على الخواص البصرية لأغشية $\text{Cu}_2\text{CdSnS}_4$ الرباعية الرقيقة

شيماء خاشع عبدو، جمال مال الله رزيج\*

قسم الفيزياء، كلية العلوم، جامعة الانبار، الانبار، العراق

### الخلاصة

السبائك الرباعية من  $\text{Cu}_2\text{CdSnS}_4$  (CCSS) هي احدى انواع الأغشية الرقيقة التي تساهم في مجالات تصنيع الأجهزة الكهروضوئية التي لم يسلط الضوء عليها بشكل واسع مثل معظم المواد. لإعداد أغشية CCSS الرقيقة عند 350 درجة سيليزية على قواعد من الزجاج، تم استخدام تقنية التخلل الكيميائي الحراري. درست الخصائص البصرية للأغشية الرقيقة المحضرة تحت تأثير تغيير مولارية محلول النحاس (0.03، 0.05، 0.07، 0.09) على المركب الرباعي باستخدام مطياف الأشعة فوق البنفسجية. أظهرت نتائج دراسة مجهر القوى الذرية ان ذرات السطح تكثفت بشكل أعمدة نانوية مع زيادة معدل الحجم الحبيبي من 62,72 إلى 79,17 نانومتر وارتفاع معدل خشونة السطح من 5,69 إلى 12,8 نانومتر عندما ازداد تركيز النحاس من

\*Email: jam72al@gmail.com

0.03 إلى 0.09 مولاري. أوضحت نتائج التحليل الطيفي أن النفاذية البصرية لأغشية CCSS تتناقص بزيادة مولارية محلول النحاس مع تغير في حافة الامتصاص نحو الأطوال الموجية الحمراء. مع زيادة الطول الموجي بين 725 و 960 نانومتر، كان معامل الامتصاص منخفضاً في منطقة الأشعة تحت الحمراء، في حين قفز بقوة في نطاق الأشعة المرئية مع زيادة مولارية محلول النحاس. انخفضت قيم فجوة الطاقة من 1.6 إلى 1.47 إلكترون فولت عندما ازدادت مولارية محلول النحاس من 0.03 إلى 0.09 مولاري. عند زيادة مولارية محلول النحاس إلى 0.09، ازداد معامل الانكسار عند حافة الامتصاص من 1.6 إلى 1.97، في حين انخفض معامل الخمود.

## 1. Introduction

The chemical and physical properties of semiconductor materials have been improved with technological advances in semiconductors. Materials were built from more powerful and cost-effective semi-conductive thin films with both the advent of nanotechnology and polymer science in the last decades [1]. Studying the deposited materials in the form of thin film is one of the most important ways to further define many chemical and physical properties of one or more layers of material atoms with a thickness not exceeding one micron [2]. In the last two decades, applications such as protection, decoration, and manufacturing of optical-electronic devices were the main industrial developments produced by thin films. Studies on the physical characteristics of thin films, such as optical properties, have been of growing interest due to a wide variety of applications in the industry [3].

Chemical spray pyrolysis (CSP) is widely used to prepare thin and thick films, semiconductor metal oxides, ceramic coatings, which is a simple and cost-effective technique. [4]. Spray pyrolysis is a thermogenic induced reaction in which the desired aqueous solution is sprayed onto the hot surface of the substrate, resulting in a single crystal or group of crystals of the compound required [5]. Thin films used in scientific and engineering fields have various practical applications as they have been used in integrated circuits, open and closed circuits, transistor production, magnetic circuit systems, amplifiers, and solar cells reagents [6]. In the field of optics, thin films are used in the profession of imaging and duplicating devices, in addition to the production of optical filters, which in turn includes the design of mirrors, anti-reflective mirrors, and edge filters [7].

Over many decades, chalcogenide semiconductors such as  $\text{Cu}_2\text{-Cd-Sn-S}$  ( $\text{Cu}_2\text{-II-IV-VI}$ ) have revived a wide range of interest in the future application of photovoltaic systems [8].  $\text{Cu}_2\text{CdSnS}_4$  (CCSS) thin films have a large absorption coefficient, low price availability, and wide energy bandgap [9]. Quaternary alloys can be deposited in a variety of methods, such as chemical vapour deposition, spray pyrolysis [10], facile solution chemistry method [11], sol-gel [12], and microwave irradiation method [13].

The objective of this research is to study the effects of copper molarity concentration on the optical properties of the  $\text{Cu}_2\text{CdSnS}_4$  chalcogenide composition, such as the transmittance, absorption coefficient, energy gap, refractive index, and extinction coefficient. Furthermore, we aim to determine the possibility of using these properties in photovoltaic and optical applications.

## 2. Experimental part

### 2.1. Materials

In the beginning, the spray solutions were prepared to obtain a quaternary film of 0.03 M copper chloride ( $\text{CuCl}_2 \cdot 2\text{H}_2\text{O}$ ), 0.02 M cadmium chloride ( $\text{CdCl}_2 \cdot 2\text{H}_2\text{O}$ ), 0.02 M tin chloride ( $\text{SnCl}_2 \cdot 2\text{H}_2\text{O}$ ), and 0.07 M thiourea ( $\text{CH}_4\text{N}_2\text{S}$ ) individually, all powders were purchased from Sigma-Aldrich Company, USA. The concentration of copper was then increased, accompanied by an increased concentration of thiourea to compensate for the loss of sulfur during the deposition, as shown in Table-1. The relation (1) was adopted [12] to calculate the weights to be dissolved to obtain the preparation solutions for the quaternary films with different copper concentrations.

$$M = \frac{w_t}{M_{wt}} \cdot \frac{1000}{V(\text{lit})} \dots \dots \dots (1)$$

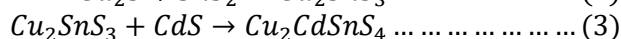
where M: solution molarity,  $M_{wt}$ : molecular weight, V: solution volume, and  $w_t$ : the required weight to be dissolved.

**Table 1**-The material, solution molarity, and weights needed for the quaternary thin film preparation solutions.

Sample	Material	Solution Molarity (mol/L)	Required Weight (gm)	Sample	Material	Solution Molarity (mol/L)	Required Weight (gm)
<b>S1</b>	CuCl <sub>2</sub>	<b>0.03</b>	0.02017	<b>S2</b>	CuCl <sub>2</sub>	<b>0.05</b>	0.03361
	CdCl <sub>2</sub>	0.02	0.01829		CdCl <sub>2</sub>	0.02	0.01829
	SnCl <sub>2</sub>	0.02	0.01899		SnCl <sub>2</sub>	0.02	0.01899
	CH <sub>4</sub> N <sub>2</sub> S	0.07	0.02664		CH <sub>4</sub> N <sub>2</sub> S	0.1125	0.04282
<b>S3</b>	CuCl <sub>2</sub>	<b>0.07</b>	0.04705	<b>S4</b>	CuCl <sub>2</sub>	<b>0.09</b>	0.0605
	CdCl <sub>2</sub>	0.02	0.01829		CdCl <sub>2</sub>	0.02	0.01829
	SnCl <sub>2</sub>	0.02	0.01899		SnCl <sub>2</sub>	0.02	0.01899
	CH <sub>4</sub> N <sub>2</sub> S	0.1575	0.05994		CH <sub>4</sub> N <sub>2</sub> S	0.2	0.07612

## 2.2. Solutions preparation

A volume of 5 ml of each solution was added with 10 ml of pure ethanol so that the overall fixed amount of the sprayed solution was 30 ml. The first step was to mix copper chloride and tin chloride solutions with a magnetic stirrer for 10 minutes, and then thiourea dropwise was added to the mixture for 30 minutes with continuous stirring at 30 ° C. In the same way, thiourea was added to the cadmium chloride solution. The resulting solution was stirred up for one hour to obtain a homogeneous, colourless, and transparent precursor solution. Equations 2 and 3 clarify the possible mechanism for the formation of Cu<sub>2</sub>CdSnS<sub>4</sub> film [14].



The precursors were sprayed at 350±5 °C on a glass substrate after being cleaned to obtain the S1 sample. While the samples S2, S3, and S4 are obtained by increasing the molarity of copper, respectively, to 0.05, 0.07, and 0.09 M. The time of spraying was (5 sec), with a stop time of (12 sec), the solution flow rate of (2 ml/min), spray distance of (29±3 cm), thin film thickness of (180±5 nm), measured by weight difference before and after deposition, and air pressure of (3 Nt/m<sup>2</sup>), were the optimum factors were used. The AFM analysis was used to analyze the morphology and topography of the thin films. The optical analysis of Cu<sub>2</sub>CdSnS<sub>4</sub> thin films was performed using a UV-Vis spectrophotometer (Lambda 900 UV-vis spectrophotometer) from 300 to 900 nm with a double beam to study absorption, optical transmittance, absorption coefficient, electronic transition, refractive index, and coefficient of extinction.

## 3. Results and discussion

### 3.1. The atomic force microscopy analysis

The analysis of surface morphology is the principal factor that can influence thin film applications. Therefore, AFM analyzes were utilized to study the surface morphology properties of the deposited thin films. Figure-1 demonstrates the topography of thin CCSS films at room temperature with various concentrations of copper. The 3D-AFM images display homogeneous distribution of atoms with grains arranged in shapes like nanorods to form a surface with valleys and hills, free from cracks and any other impurities, which suggests uniform nanoparticle granular growth.

The sharpness and number of hills on the surface increased with increasing copper concentration, accompanied by enhancement of the columnar structure, as revealed by the 3D micrographs. This can be attributed to the growth and nucleation of the grains during the crystallization process. This, in turn, leads to an increase in the average grain size (Gs) [15]. The Gs was increased from 62,72 to 79,17 nm as the concentration of copper raised from 0,03 to 0,09 M. Also, the average surface roughness increased from 5,69 to 12,8 nm, as shown in Figure-2. The formation of valleys and hills on the surface of the prepared films, as well as the increase in the grain size and surface roughness, render these types of films having effective surfaces that can be utilized in the fields of gas sensors and photodetectors [16]

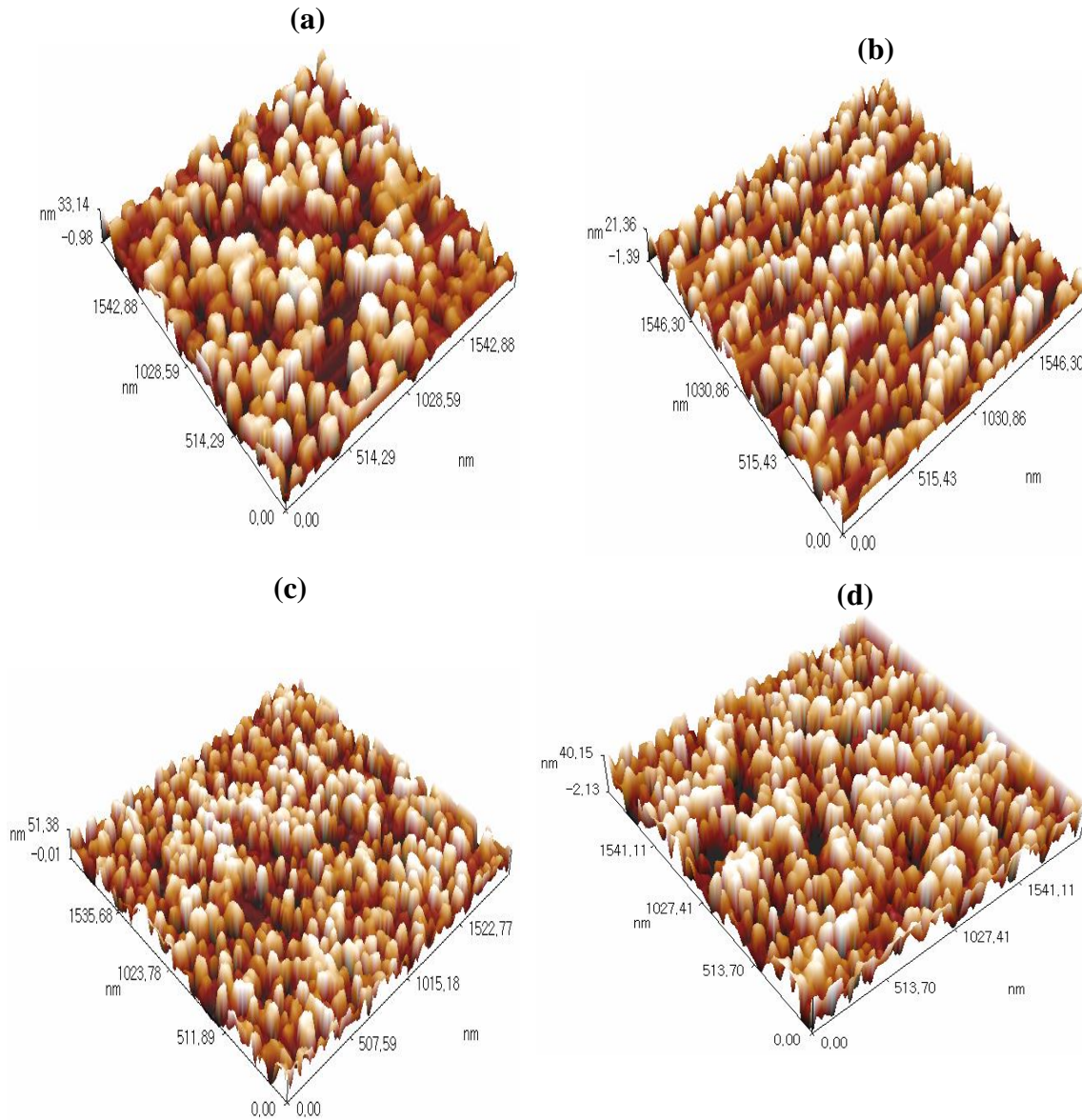


Figure 1-The 3d-AFM images of CCSS: (a) 3% Cu, (b) 5% Cu, (c) 7% Cu, and (d) 9% Cu thin films.

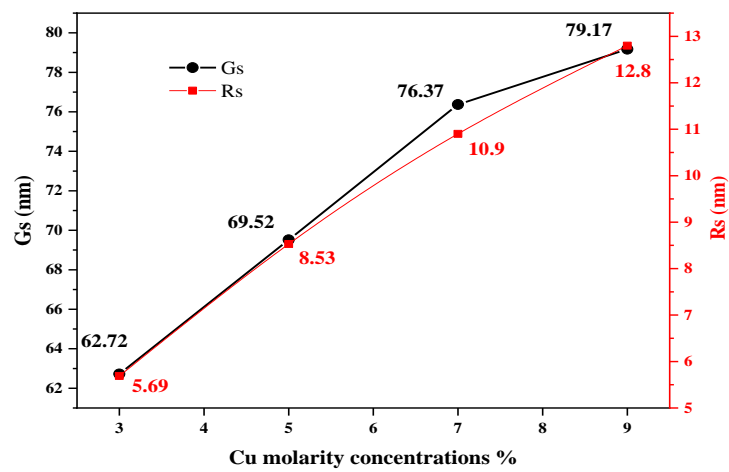


Figure 2- Average grain size (Gs) and average roughness (Rs) as a function of the Cu concentrations

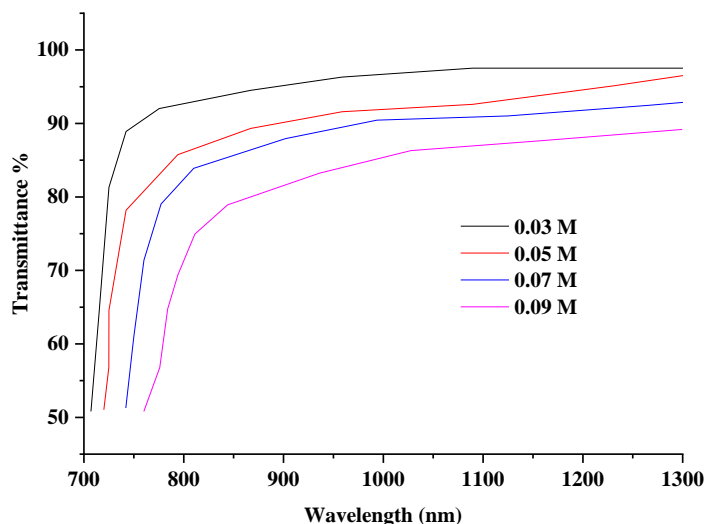
### 3.2. Transmittance

Figure-3 displays the transmittance spectrum (T%) of CCSS thin films at room temperature between 300 and 900 nm, determined from the absorption spectrum based on the following equation (4): [10]

$$T = \exp^{-2.303 A} \quad \dots \dots \dots (4)$$

where  $T$  is the transmittance and  $A$  is the absorbance.

Figure-3 shows that the lowest transmittance was 50% for the S1 sample at 707 nm ( $\lambda_{min}$ ) that is close to the initial absorption edge, which was rapidly increased to 82% at the absorption edge ( $\lambda_{edg}$ ), while it had a maximum value of 97% at the end of the spectrum ( $\lambda_{max}$ ), as shown in Table-2.



**Figure 3-**Transmittance spectrum as a function of the wavelength for S1, S2, S3 and S4 samples.

Based on Figure-3, the T% of the samples S2, S3, and S4 decreased when copper solution molarity increased to reach a lower transmittance of 89% for the sample S4 at 1300 nm and the absorption edge being changed toward the long-wavelength (redshift). The decrease in the optical transmittance can be explained by the improvement in the optical absorption rate. This can be due to the increase in the average grain size and the decrease in granular boundaries, with the increase in copper solution molarity [17], as mentioned in AFM results and Figure-2. These films may be used in electronic applications, as in the optical windows that have effective regions within the visible spectrum range. The prepared films with low transmittance at the edge of the absorption spectrum can also be used as a reflective coating to cover the windows of high-rise buildings in relatively high-temperature regions.

**Table-2** tabulates the values of transmittance at ( $\lambda_{min}$ ), ( $\lambda_{edg}$ ), and ( $\lambda_{max}$ ) for four samples.

Cu molarity (M)	$\lambda_{min}$ (nm)	T%	$\lambda_{edg}$ (nm)	T%	$\lambda_{max}$ (nm)	T%
0.03	707	53	720	82	1300	97
0.05	720	52	729	78	1300	95
0.07	742	51	756	71	1300	93
0.09	760	50	800	69	1300	89

**Table 2-**Transmittance at  $\lambda_{min}$ ,  $\lambda_{edg}$  and  $\lambda_{max}$  of the CCSS thin films prepared by CSP

### 3.3. Absorption coefficient ( $\alpha$ )

Figure-4 shows the change in the absorption spectrum ( $\alpha$ ) as a function of the wavelength within the wavelength range from 300 to 900 nm. In practice, the absorption coefficient ( $\alpha$ ) was determined using equation (5) by measuring both the absorption ( $A$ ) and the transmittance ( $T$ ) as in the following:[18]

$$\alpha = 2.303 \frac{A}{t} \quad \dots \dots \dots (5)$$

Figure-4 shows that the S1 sample had a low absorption coefficient in the infrared spectrum, whereas it was high in the visible range. A significant decrease in the absorption coefficient was observed with the wavelength between 725 and 960 nm.

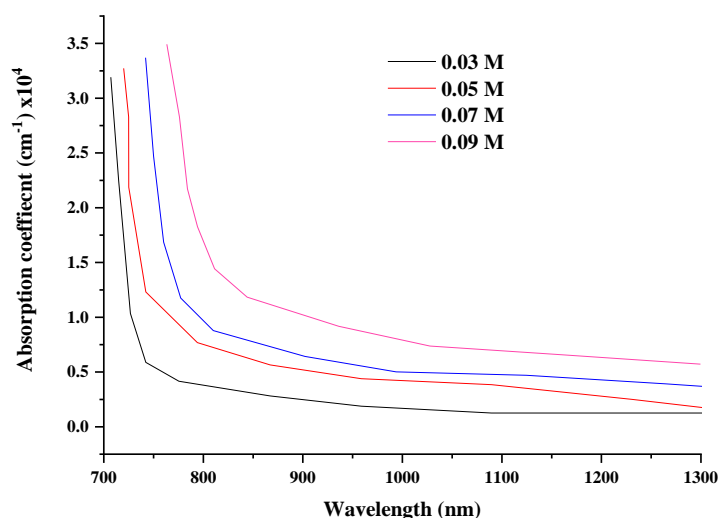


**Figure 4-** Absorption coefficient spectrum as a function of the wavelength for the CCSS thin films prepared by CSP.

This effect leads to an increase in optical transmittance within this range of the electromagnetic spectrum. The stability of the absorption coefficient is observed with the increase in wavelength within the spectral range of 960-1300 nm. This is because of the relative stability of the transmittance rate within this region. In other words, there is a limited chance of electronic transformations in this spectral region since the energy of the photon is less than the value of the energy gap, so that the absorption coefficient in this spectrum is decreased with increasing wavelength [18].

Figure-4 also shows that the absorption coefficient increased with increasing copper solution molarity from 0.03 to 0.09 M to reach the maximum value for the sample S4, as shown in Table-3. The explanation for this result may be that the increase in copper solution molarity led to an increase in crystal defects and an increase in the localization of the state within the energy gap. This is confirmed by the results of the tail width of the localized states calculations, which in turn led to an increase in the number of electronic transitions between the valence and the conductive band [19]. Table-3 shows that the absorption coefficient values for all the prepared films were higher than  $10^4$ , which gives the initial impression that the prepared films have a direct energy gap [20]. Thus, these films can be used as absorbent sunscreens on building windows, i.e., as selective radioactive filters to track radiation [21].

**Table 3-**Absorption coefficient at  $\lambda_{\min}$ ,  $\lambda_{\text{edg}}$  and  $\lambda_{\max}$  of the CCSS thin films

Cu molarity (M)	$\lambda_{\min}$ (nm)	$\alpha \times 10^4$ ( $\text{cm}^{-1}$ )	$\lambda_{\text{edg}}$ (nm)	$\alpha \times 10^4$ ( $\text{cm}^{-1}$ )	$\lambda_{\max}$ (nm)	$\alpha \times 10^4$ ( $\text{cm}^{-1}$ )
0.03	1300	1.25	720	1.03	707	3.19
0.05	1300	1.72	729	1.17	720	3.27
0.07	1300	3.44	756	1.23	742	3.36
0.09	1300	5.72	800	1.44	763	3.49

### 3.4. Energy gap ( $E_g$ )

In semiconductor physics, the optical energy gap is a major constant considering the promise of the semi-conducting materials to be used in various optoelectronic applications [22]. One of the factors affecting the energy gap is the type of the prepared thin film and its preparation method, which is greatly affected by the deposition temperature and material concentration. In addition, the energy gap

is influenced by the preparation conditions, nature of the crystal structure, and how atoms are distributed in the crystal lattice [23]. The energy gap was calculated by the relation (6): [24]

$$ahv = B(hv - E_g)^r \dots \dots \dots (6)$$

where  $E_g$  is the optical energy gap in eV,  $h\nu$  is the absorbed energy photon,  $B$  is a constant that depends on the nature of the material, and  $r$  is the exponential coefficient that depends on the nature of the transitions. The results of the energy gap calculations are shown in Figure-5a, which is determined by drawing the relation between  $(ah\nu)^2$  as a function of the photons energy ( $h\nu$ ), where  $(r = \frac{1}{2})$ .

In addition, the tail width of the localized states was calculated using equation (7) [25] and Figure-5b.

$$\alpha = \alpha_o \exp\left(\frac{h\nu}{E_e}\right) \dots \dots \dots (7)$$

where  $\alpha_o$  is the correlation constant and  $E_e$  is the tail width of the localized states within the optical energy gap. The latter can be calculated from the reciprocal  $\ln(\alpha)$  with  $h\nu$  slope.

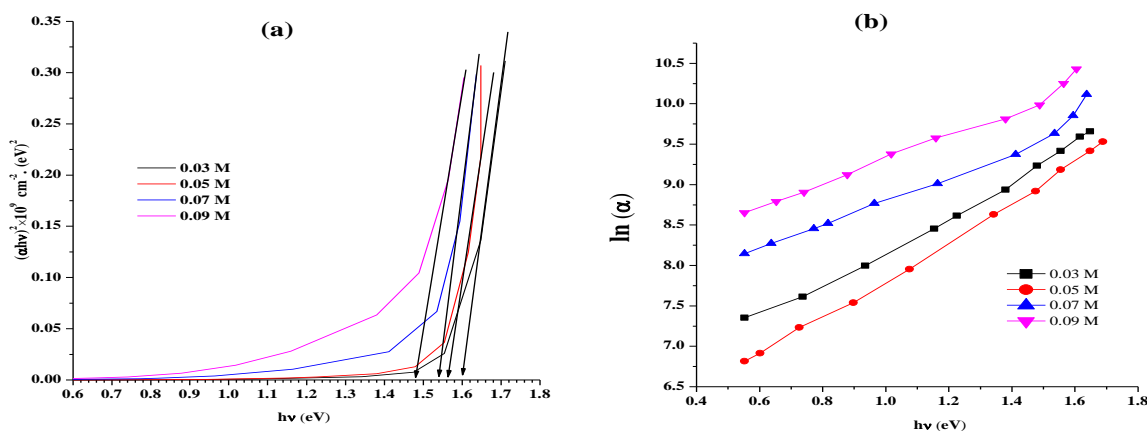


**Figure- 5 (a)** Energy gap as a function of the photon energy and (b) the band tails as a function of the photon energy for the CCSS thin films.

The  $E_g$  results revealed that all the prepared films have a direct electronic transition type, as expected from the absorption coefficient measurement. Table-4 shows that the S1 sample has an energy gap at room temperature equal to 1.66 eV, in agreement with the results obtained by an earlier report [10]. When copper solution molarity was raised to 0.05, 0.07, and 0.09, respectively, the energy gap was decreased to 1.57, 1.55, and 1.47 eV.

Figure-5b shows the variation of  $\ln(\alpha)$  as a function of the incident photon energy, through which the width of the tails was determined for the localized energy states, as listed in Table-4. From this table, it is noted that the increase in copper concentration increases the width of the tails, which affects the values of the absorption coefficient in addition to the energy gap values.

**Table 4-** The variation of energy gap with Cu molarity concentration and tail width of the localized states within the energy gap of the CCSS thin films prepared by CSP.

Cu molarity (M)	Energy gap (eV)	slope	Tail width (eV)
0.03	1.6	2.3777	0.4205
0.05	1.56	2.156	0.4638
0.07	1.53	1.6598	0.6024
0.09	1.47	1.5757	0.6346

The reduction in the energy gap with the rising copper concentration can be due to an increase in the absorption coefficient. It can also be explained by the energy tail broadening with the increase of

the copper concentration, as shown in Table-4. The increase in copper concentration contributes to the creation of donor states near the conductive band inside the energy gap, then the Fermi level is shifted toward the conductive band, and the photons with energy below 1.6 eV will be absorbed [20]. Since the prepared films have an energy gap that matches that suitable for photovoltaic devices, they can be used with high efficiency in this field [10].

**3.5. The refractive index**

For CCSS thin films, the refractive index (n) values were obtained using equation (8): [12]

$$n = \frac{1+\sqrt{R}}{1-\sqrt{R}} \dots \dots \dots (8)$$

where R is the reflectance of the thin film; it is the ratio of the light velocity in the vacuum to its medium velocity. Figure-6 displays the curves of (n) as a function of wavelength. The refractive index value for sample S1 at wavelengths of 725 to 960 nm is decreased significantly, followed by a relative decrease after this spectrum. This may be due to a change in the distribution of atoms on the thin film surface and then in the roughness of the film, in accordance with previously published results [26].

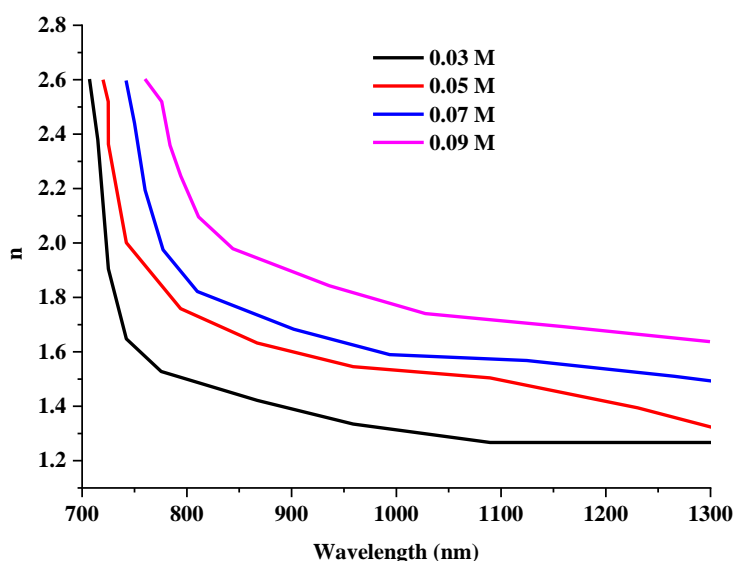


**Figure 6-**The variation of refractive index with the wavelength of the CCSS thin films.

Table-5 shows that, at the beginning of the spectrum, the maximum refractive index was around 2.6, whereas at the absorption edge, it was 1.6, and at the end of the spectrum, it was 1.26 as the lowest value. Figures 4 and 6 display the same behaviour; by raising the copper molarity solution, the refractive index was increased at the edge of absorption to 1.97 for the S4 sample. This may be due to the fact that increasing the concentration of copper increases the size of the grain, which makes the film surface denser and, consequently, reduces the speed of light diffusion through it [15].

**Table 5-**The refractive index at  $\lambda_{min}$ ,  $\lambda_{edg}$  and  $\lambda_{max}$  of the CCSS thin films prepared by CSP.

Cu molarity (M)	$\lambda_{min}$ (nm)	n	$\lambda_{edg}$ (nm)	n	$\lambda_{max}$ (nm)	n
0.03	1300	1.26	720	1.6	707	2.6
0.05	1300	1.31	729	1.75	720	2.6
0.07	1300	1.47	756	1.82	742	2.6
0.09	1300	1.63	800	1.97	763	2.6

The refractive index values obtained for the quaternary alloy thin films appear to be very suitable for their utilization in photo conversion and optoelectronic devices, as they have a high absorption coefficient and a low refractive index, which increases the efficiency of these devices [27].

### 3.6. The extinction coefficient

The extinction coefficient (K) represents the energy absorbed in the film. It was calculated from relation (9): [12]

$$k = \lambda\alpha/4\pi \dots \dots \dots (9)$$

where  $\lambda$  is the wavelength of the incident photon.

Figure-7 indicates the extinction coefficient variation with wavelengths from 715 to 1300 nm. It shows similar behaviour to that of the absorption coefficient because of the close relationship between them shown in relation (9).

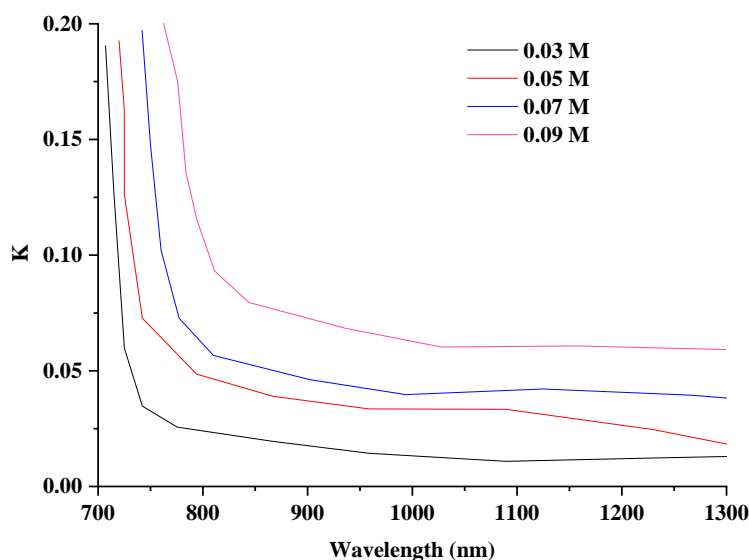


**Figure 7-**The extinction coefficient variation as a function of wavelength of the CCSS thin films.

Figure-7 shows a rapid decrease in  $k$  at the UV-visible range, followed by relative stability within the visible spectrum region with a wavelength increase, which is a general behaviour for all the prepared films. However, this variance of the extinction coefficient depends on several factors; basic type of surface film formation, roughness and density, distribution of atoms, nature of the nanostructure, etc. [28]. The increase in the molarity of the copper solution increased the extinction coefficient. This increase was caused by the amount of attenuated radiation on the thin film surface [29]. Figure-7 also shows that the extinction coefficient has the highest values within the short wavelength region due to the fact that the fundamental absorption falls within this region, which indicates the amount of radiation energy loss. In other words, the higher frequency of the incoming photon, the higher probability of absorption. The low  $k$  at long wavelengths could be due to the increased transmittance of the prepared films within this spectral range [30]. Table-6 indicates the rate of the extinction coefficient of all films prepared at various wavelengths.

**Table 6-**The extinction coefficient at  $\lambda_{min}$ ,  $\lambda_{edg}$  and  $\lambda_{max}$  of the CCSS thin films prepared by CSP.

Cu molarity (M)	$\lambda_{min}$ (nm)	$k$	$\lambda_{edg}$ (nm)	$k$	$\lambda_{max}$ (nm)	$k$
0.03	1300	0.013	720	0.024	707	0.19
0.05	1300	0.017	729	0.028	720	0.192
0.07	1300	0.036	756	0.033	742	0.196
0.09	1300	0.059	800	0.057	763	0.2

### 4. Conclusions

Thin films of the quaternary  $Cu_2CdSnS_4$  were deposited successfully using the spray pyrolysis method. As the prepared films have high optical transmission, they can be utilized in the field of optical window applications. CCSS thin films can be used as absorbent sunscreens on windows, i.e.,

selective radioactive filters for radiation detection since they have a high absorption factor. UV–vis analysis also indicated that the optical band gaps are very close to the optimum. The prepared thin films can be very suitable for photo conversion and optoelectronic devices, according to the refractive index and the extinction coefficient results.  $\text{Cu}_2\text{CdSnS}_4$  films with different copper concentrations can also be used as effective surfaces in gas sensors and optical detector devices, as they have appropriate characteristics for these applications.

## Reference

1. Rudan M. **2018**. *Physics of Semiconductor Devices*. Second Edition. Springer International Publishing.
2. Glynn C., O'Dwyer C. **2017**. Solution Processable Metal Oxide Thin Film Deposition and Material Growth for Electronic and Photonic Devices, *Advanced Materials Interfaces*, 4(2), pp:1600610–46.
3. Sönmezolu S., Arslan A., Serin T., Serin N. **2011**. The effects of film thickness on the optical properties of  $\text{TiO}_2$ - $\text{SnO}_2$  compound thin films, *Physica Scripta*, 84(6), pp:1–6.
4. Ali IM, Rzaij JM, Abbas QA, Ibrahim IM, Alatta HJ. **2018**. Structural, Optical and Sensing Behavior of Neodymium-Doped Vanadium Pentoxide Thin Films, *Iranian Journal of Science and Technology, Transactions A: Science*, 42(4), pp:2375–2386.
5. SINGH DVK. **2017**. Thin Film Deposition by Spray Pyrolysis Techniques, *Emerging Technologies and Innovative Research (JETIR)*, 4(11), pp:1–9.
6. Khanlary MR, Alizade F, Malekfar R. **2020**. Optical and structural investigation of  $\text{ZnS}:\text{Cu}$  thin films synthesized by spray pyrolysis, *Optical and Quantum Electronics*, 52(5), pp:237–250.
7. Wielgosz R, Kulyk B, Turko B, Chtouki T, Kapustianyk V, et al. **2019**. Nanostructured  $\text{CuO}$  thin film for nonlinear optical applications, 21<sup>st</sup> International Conference on Transparent Optical Networks, July 9-13, Angers, France.
8. Su Z., Tan JMR, Li X., Zeng X., Batabyal SK, et al. **2015**. Cation Substitution of Solution-Processed  $\text{Cu}_2\text{ZnSnS}_4$  Thin Film Solar Cell with over 9% Efficiency, *Advanced Energy Materials*, 5(19), pp:2–8.
9. Shavel A, et al. **2012**. ChemInform Abstract:  $\text{Cu}_2\text{ZnGeSe}_4$  Nanocrystals: Synthesis and Thermoelectric Properties, *ChemInform*, 43(25), pp:4060–63.
10. Rouchdi M., Salmani E., Hassanain N., Mzerd A. **2017**. Effect of deposition time on structural and physical properties of  $\text{Cu}_2\text{CdSnS}_4$  thin films prepared by spray pyrolysis technique: experimental and ab initio study, *Optical and Quantum Electronics*, 49(4), pp:165–177.
11. Y.FL, M. YG, H. HL, Y. S, J. W, et al. **2012**. Synthesis and properties of colloidal  $\text{Cu}_2\text{CdSnS}_4$  nanocrystals, *Hongwai Yu Haomibo Xuebao/Journal of Infrared and Millimeter Waves*, 31(1), pp:1–4.
12. Al-Douri Y., Odeh AA, Johan MR, Chowdhury ZZ, Rafique RF, et al. **2018**. Synthesis and characterization of  $\text{Cu}_2\text{CdSnS}_4$  quaternary alloy nanostructures, *International Journal of Electrochemical Science*, 13(7), pp:6693–6707.
13. Guan H, Shi Y, Hou H, Wang X, Yu F. **2014**. Quaternary  $\text{Cu}_2\text{CdSnS}_4$  nanoparticles synthesised by microwave irradiation method, *MICRO AND NANO LETTERS*, 9(4), pp:251–252.
14. Guan H., Zhao J., Wang X., and Yu F. **2013**.  $\text{Cu}_2\text{CdSnS}_4$  thin film prepared by a simple solution method, *Chalcogenide Lett.* 10(10), pp:367–372.
15. Hojabri A. **2016**. Structural and optical characterization of  $\text{ZrO}_2$  thin films grown on silicon and quartz substrates, *Journal of Theoretical and Applied Physics*. 10(3), pp: 219–224.
16. Rzaij JM, Habubi NF. **2020**. Room temperature gas sensor based on  $\text{La}_2\text{O}_3$  doped  $\text{CuO}$  thin films, *Appl. Phys. A*. 126(7), pp:560–570.
17. Mohamed JR, Amalraj L. **2016**. Effect of precursor concentration on physical properties of nebulized spray deposited  $\text{In}_2\text{S}_3$  thin films, *Journal of Asian Ceramic Societies*, 4(3), pp:357–366.
18. Hasan BA, Rzaij JM, Ali IM. **2016**. Sensing Properties of  $(\text{In}_2\text{O}_3:\text{Eu})$  Thin Films, *Australian Journal of Basic and Applied Sciences*, 10(8), pp:143–150.
19. Mo LB, Bai Y., Xiang QY, Li Q., Wang JO, et al. **2014**. Band gap engineering of  $\text{TiO}_2$  through hydrogenation, *Applied Physics Letters*, 105(20), pp:20–24.
20. Rzaij JM. **2016**. Characterization of  $\text{CuO}$  thin films for gas sensing applications, *Iraqi Journal of Physics*, 14(31), pp:1–12.

21. Rzaïj JM, Ibrahim IM, Alalousi MA, Habubi NF. **2018**. Hydrogen sulfide sensor based on cupric oxide thin films, *Optik - International Journal for Light and Electron Optics*, 172, pp:117–126.
22. Jothi S., Prithivikumaran N., Jeyakumaran N. **2014**. Optical parameter determination of ZrO<sub>2</sub> thin films prepared by sol gel dip coating, *International Journal of ChemTech Research*, 6(13), pp:5342–5346.
23. Yahya KZ, Haider AJ, Tarek HS, Al-Haddad RM. **2014**. Effect of Substrate Temperature on Nanostructure Titanium Dioxide Thin Films Prepared by PLD, *Eng & Tech Journal*, 32(3), pp:3–4.
24. Latif NT, Rzaïj JM. **2020**. Concentration Effect of Mixed SnO<sub>2</sub>-ZnO on TiO<sub>2</sub> Optical Properties Thin Films prepared by Chemical Spray Pyrolysis Technique, *J. Univ. Anbar pure Sci*, 14(1), pp:43-49
25. Al-dileamy MN, Alnaimi SM. **2004**. Films Prepared by Chemical Spray Pyrolysis Technique, *Qatar Univ. Sci. J.*, 24, pp:79–90.
26. Bouachiba Y., Bouabellou A., Hanini F., Kermiche F., Taabouche A., *et al.* **2014**. Structural and optical properties of TiO<sub>2</sub> thin films grown by sol-gel dip coating process, *Materials Science-Poland*, 32(1), pp:1–6.
27. Usha KS, Sivakumar R., Sanjeeviraja C. **2015**. Effect of substrate temperature on structural and optical properties of nickel tungsten oxide thin films, *Journal of Materials Science Materials in Electronics*, 26(2), pp:1033–1044.
28. Sta I., Jlassi M., Hajji M., Boujmil MF, Jerbi R., *et al.* **2014**. Structural and optical properties of TiO<sub>2</sub> thin films prepared by spin coating, *Journal of Sol-Gel Science and Technology*, 72(2), pp:421–427.
29. C. HT, P. HF, C. ML, S. LS. **2018**. CuO and CuO/graphene nanostructured thin films as counter electrodes for Pt-free dye-sensitized solar cells, *Coatings Coatings*, 8(21), pp:1–13.
30. Tash-toush NM, Sheiab A., Jafar M., Momani S. **2019**. Determining Optical Constants of Sol-Gel Vanadium Pentoxide Thin Films using Transmittance and Reflectance Spectra, *International Journal of Physics: Study and Research*, 2(1), pp:59–64.